Non-Dispersive Ultra-Violet Spectroscopic Detection of Formaldehyde Gas for Indoor Environments

J. J. Davenport, J. Hodgkinson, J. R. Saffell, and R. P. Tatam

***Abstract*— We describe a simple method for detecting formaldehyde using low resolution non-dispersive UV absorption spectroscopy. A two channel sensor was developed, making use of a strong absorption peak at 339 nm and a neighboring region of negligible absorption at 336 nm as a reference. Using a modulated UV LED as a light source and narrow laser-line filters to select the desired spectral bands, a simple detection system was constructed specifically targeted at formaldehyde. By paying particular attention to sources of noise, a minimum detectable absorbance of 5×10^{-5} absorbance units (AU) was demonstrated with a 20 s averaging period (as $\Delta I/I_0$). The system was tested with formaldehyde finding a limit of detection of 4.3 ppm for a 195 mm gas cell. As a consequence of the low gas flow rates used in our test system, a time period of over 8 min was used in further tests, which increased the minimum detectable absorbance to 2×10^{-4} AU, 17 ppm of formaldehyde. The increase was the result of thermal drift caused by unwanted temperature variation of the UV LED and the filters, resulting in a zero uncertainty estimated at -560 ppm $^{\circ}C^{-1}$ and 100 ppm $^{\circ}C^{-1}$ respectively.**

***Index Terms*— Gas detectors, light emitting diodes, optical sensors, pollution measurement, spectroscopy, ultraviolet sources.**

I. Introduction

FORMALDEHYDE, also known as methanal, methyl aldehyde and methylene oxide, is the first member of the aldehyde chemical family and has the chemical formula CH_2O. Under standard conditions it is a colourless gas which is toxic, allergenic and a potential human carcinogen [1]–[3]. It has been shown to cause inflammation of lung epithelial cells [4] and to be dangerous at the ppb level (parts-per-billion, 1 molecule in 10^9 of air) [5]. The World Health Organisation (WHO) has set a guideline level for prolonged formaldehyde exposure at 80 ppb over a 30 minute period, and many countries have set their limits in line with this [6], [7]. Some countries have different guideline levels over different time periods, for example the limits for Singapore and South Korea are 0.1 ppm over 8 hours [7].

Formaldehyde is also a valuable industrial chemical with limited alternatives [1], [2], [7]. Formaldehyde resin is used as an adhesive in plywood [8], [9] and in carpeting [10], and is also used in the production of paints [11] and wallpapers [12]. Emission levels are highest when products are new, generally decreasing exponentially, but can take several years to reach safe levels [6], [7], [13]. As a result formaldehyde gas can often build up in enclosed areas and, particularly when new furnishings or carpeting have been installed, it can pose a serious health risk.

Biochemical formaldehyde sensors, such as 'bio-sniffers' [6], can be highly sensitive but can be difficult to implement as standalone sensors. For example, the sensor of Kudo *et al*. [6] requires circulation of a chemical reagent and pH buffer for correct operation, which precludes its use as a compact sensor for field use requiring minimal human intervention. An electrochemical gas sensor is also available [14], however electrochemical sensors are known to have limited lifetimes and can suffer from cross-response to other gas species and humidity. Thin film sensors, including semiconductor sensors, can show ppb level sensitivity but suffer from cross-response to humidity and other indoor gases [15].

Optical sensors generally offer a number of advantages for gas detection including fast response times, reliable components and, for absorption based sensors, non-contact operation. They typically work by the principle of spectroscopy, wherein light is passed through a sample and its resultant absorption spectrum is used to identify and quantify gases present [16].

In tunable diode laser spectroscopy (TDLS), a diode laser's wavelength is tuned to scan across the absorption spectrum of the target gas. Quantum cascade lasers (QCLs), inter-band cascade lasers (ICLs) or difference frequency generation (DFG) sources enable access the mid infrared region where linestrengths are greater than those in the near IR, and sensitivity can be further improved by the use of multipass gas cells such as Herriott cells [16]. In the mid IR (near 3.5μm) Wysocki *et al*. [17] demonstrated a detection limit of 3.5 ppb with a response time of 1 s and Richter *et al*. [18] achieved a limit of 74 ppt but with increased response time (once per minute). Sensitivity can be further improved by the use of cavity-enhanced techniques, for example enabling

Manuscript received October 26, 2017; revised December 23, 2017; accepted January 4, 2018. Date of publication January 25, 2018; date of current version February 21, 2018. This work was supported by the U.K. Engineering and Physical Sciences Research Council under Grant GR/T18424, EP/P504880 and Grant EP/H02252X. The associate editor coordinating the review of this paper and approving it for publication was Dr. Chang-Soo Kim. *(Corresponding author: J. Hodgkinson.)*

J. J. Davenport was with Engineering Photonics, Cranfield University, Cranfield MK43 0AL, U.K. He is now with the Research Centre for Biomedical Engineering, City, University of London, London EC1V 0HB, U.K. (e-mail: john.davenport.1@city.ac.uk).

J. Hodgkinson and R. P. Tatam are with Engineering Photonics, Cranfield University, Cranfield MK43 0AL, U.K. (e-mail j.hodgkinson@cranfield.ac.uk; r.p.tatam@cranfield.ac.uk).

J. R. Saffell is with Alphasense Ltd., Great Notley CM77 7AA, U.K. (e-mail: jrs@alphasense.com).

Digital Object Identifier 10.1109/JSEN.2018.2795042

measurement of weaker absorption lines in the near infrared region at 1.76 μm [19]. TDLS systems demonstrate good species selectivity, often with no spectral overlap between absorption lines, and excellent signal-to-noise ratios, but can be expensive and / or complex to manufacture.

Photoacoustic spectroscopy (PAS) relies on the photoacoustic effect whereby sound is produced by the absorption of light from a modulated source. PAS has been shown to give good sensitivity and response time (detection of 3 ppb formaldehyde at one measurement per three minutes being shown by Angelmahr *et al*. [20]) but can be susceptible to background acoustic noise. The QEPAS technique, as demonstrated by Horstjann *et al.* [21] for formaldehyde , aims to solve this problem using a quadrupole acoustic sensor, however to sensitively detect formaldehyde still requires a costly ICL source. Finally a commercial rack-mounted instrument is available based on the photoacoustic principle used with a QCL source, giving a sub ppb detection limit [22].

Differential optical absorption spectroscopy (DOAS) is commonly used for outdoor formaldehyde detection, consisting of a light source, a long path arrangement often traveling hundreds of metres through the atmosphere, and a high resolution (sub nanometre) spectrometer [23]–[26]. Stutz and Platt [27] have published algorithms required to separate measurements of concentrations of ozone, nitrogen dioxide, sulfur dioxide and formaldehyde in the atmosphere. Hausmann *et al*. [28] estimated the error when using UV DOAS to measure OH, SO_2, $C_{10}H_8$ and formaldehyde in the atmosphere, in the presence of instrumental noise. Both papers reveal a high degree of complexity in the spectral post-processing required to separate these species at trace atmospheric levels using their UV absorption spectra.

Also in the UV, Washenfelder *et al.* [29] have developed a broadband cavity-enhanced detector for formaldehyde and nitrogen dioxide, using the 310-360 nm region, a broadband, laser diode-pumped xenon lamp and a grating spectrometer. High reflectivity mirrors enabled a 1.43 km effective cavity length within a physical distance of 1m. Detection limits were 140 and 210 ppt for CH_2O and NO_2 respectively. While such instruments perform well, their size and complexity makes them unsuited to hand-portable field measurements.

We have previously shown that the region of the formaldehyde absorption spectrum between 320 and 360 nm has relatively little interference from other indoor gases [30]. 85 chemicals and chemical groups common to the indoor environment were identified, 32 of which had absorption spectra in the UV-Vis region. Of these, 11 were found to overlap with the formaldehyde UV region. It was found that the region between 320 to 360 nm is relatively free from interference from indoor gases, with NO_2 being the only major interferent. Although other gases such as acetaldehyde also have the potential to interfere, their concentrations in the indoor environment are so low in comparison that in practice the level of such interference would be negligible.

Within this region are bands with high absorption from formaldehyde and regions of minimal absorption (see Fig. 1). This makes the region suitable for a low resolution, two channel spectroscopy system specifically targeted at formaldehyde

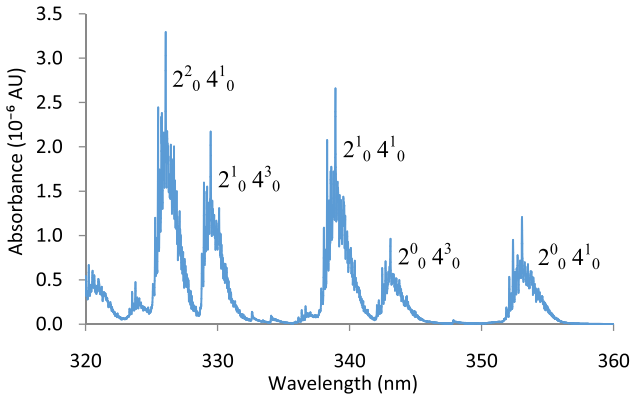

Fig. 1. Absorbance of formaldehyde in the identified region, assuming a 10 ppb concentration and a 100 mm path length, calculated from data from Meller and Moortgat [32]. The major vibration state peaks are marked [33]. This region has relatively little interference from gases common to the indoor environment [30].

absorption features. For such a scheme, 32 ppb of NO_2 was estimated to have a cross-sensitivity with equivalent magnitude to 100 ppb of formaldehyde [30]. In principle, this problem would be avoided by the use of a commercially available NO_2 sensor, or use of a third detection channel targeting NO_2.

Here, a two channel system is demonstrated using a single UV LED as a light source and a pair of laser-line bandpass filters to give a measurement and a reference channel. The performance and engineering compromises resulting from this choice of components, and performance limitations, are discussed.

II. Theory of Operation

The degree of absorption through a given sample is governed by the Beer-Lambert law shown in [31, eq. (1)].

$$\frac{I(\lambda)}{I_0(\lambda)} = e^{-\sigma(\lambda) l N} \tag{1}$$

where I is the final intensity of light transmitted through a sample at wavelength λ, I_0 is the initial intensity at that wavelength, σ is the absorption cross-section per molecule of absorbing gas at that wavelength, l is the light path length through the sample and N is the number density of absorbing gas molecules.

At low values of $\sigma\ l\ N$, this approximates to a linear relationship as follows:

$$I \approx I_0\ (1\ -\ \sigma(\lambda) l N) \tag{2}$$

We can define the *absorbance* of a sample as the ratio of absorbed intensity to initial intensity:

$$\frac{\Delta I(\lambda)}{I_0(\lambda)} = \frac{I(\lambda) - I_0(\lambda)}{I_0(\lambda)} \tag{3}$$

The sensitivity of a spectroscopy device can be quantified as its *noise equivalent absorbance* (NEA), with dimensionless units AU (absorbance units). This is the absorbance at which the signal, as $\Delta I/I_0$, is equal to the RMS noise, and is independent of pathlength.

The 320-360 nm region of the formaldehyde spectrum is repeated in Fig. 1 re-plotted from data measured by

Meller and Moortgat [32]. The major vibrational absorption peaks are labelled, following the form M^a_b for a transition of the vibration state M, a and b representing the quantum numbers in the upper and lower energy states respectively [33].

The instrument was built to use two wavelength bands, one for the reference channel and one for the signal channel/band. The detection band was centered at 339 nm and the reference band centered at 336 nm. It used the $2^1_0 4^1_0$ formaldehyde absorption peak, one of the strongest formaldehyde absorption peaks in the region.

For a broadband measurement, transmission through the detection channel comprises the integrated gas absorption:

$$I = I_0 \int E_S(\lambda)\ T(\lambda)\ \exp[-\sigma(\lambda) l N]\mathrm{d}\lambda \tag{4}$$

Where E_s is the emission envelope of the source and T is the transmission of the detection channel filter. In the region of linear operation, we can adapt (2) to give the absorbance;

$$\sigma' l N = 1 - \frac{I_D}{I_{0D}} \tag{5}$$

where the subscript D denotes the detection channel, and σ' is a pseudo absorption cross-section that follows from (4). The performance of non-dispersive systems can be estimated in terms of the minimum detectable change in optical power, $\Delta I/I_0$. For non-dispersive spectroscopy the figure corresponds to a noise equivalent absorbance (NEA) where the "absorbance" concerned is an integrated effective absorbance over the measurement band.

A reference channel is used to compensate for changes in the emission of the source, which are assumed to affect the reference and active channel wavelengths in equal proportion. Thus, we measure the reference channel intensity I_{R} as a substitute for I_0 and define the normalized absorbance signal S as;

$$S = 1 - \frac{I_{0R}}{I_{0D}} \frac{I_D}{I_R} \tag{6}$$

where the subscript R denotes the reference channel. S is unitless but typically described in "absorbance units" (AU). The value of $I_{0\mathrm{R}}/I_{0\mathrm{D}}$ may be determined by flushing the sample cell with clean air. In our results below we report this normalized absorbance, S, corrected for drift using the reference channel.

III. System Design

A. Optical Configuration

The system used two channels for detection and reference respectively, defined by narrowband filters described in section section III.B. The channels were selected to be sufficiently close to be able to use a single LED as a light source.

A diagram of the optical setup is shown in Fig. 2. We used a 340 nm UV LED (SETi UVTOP335TO39BL) with an emission bandwidth of 15 nm (FWHM), which incorporated a parabolic reflector in the package and therefore produced a partially collimated beam of light. This was further collimated into the 195 mm long gas cell by a 60 mm focal length lens (NA: 0.30). A 50:50 beam splitter divided the light into two channels. Light from each channel then passed through a custom made laser-line filter, angled to tune the transmission wavelength to the desired range. Finally, the light within each channel was focused by a 16 mm focal length lens (NA 0.63) onto a photodiode for detection (RS Components OSD5.8-7QSD5.8-7Q).

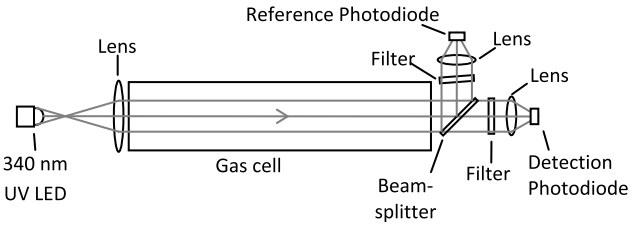

Fig. 2. Diagram of the optical system. Light from a 340 nm LED was collimated through the gas cell before being divided into a detection channel and a reference channel. The desired spectral range was then selected by the filters before the light was focused onto the photodiodes for detection.

B. Laser-Line Filters

While it was not necessary to distinguish the sub-nanometre spectral features of the formaldehyde spectrum, the main bands still had relatively narrow widths of around 3 nm. Commercially available 'narrow' band-pass filters had typical transmission bandwidths of 10 nm, which was too wide for the purpose of this system. 'Laser-line' filters presented a better prospect, typically having transmission bandwidths of between 2 and 3 nm. These filters are designed to permit transmission from a specific laser emission wavelength but block other wavelengths, and have precisely defined transmission spectra.

Like most band-pass filters, laser-line filters work on the principle of optical interference via a number of thin film layers that are deposited on the filter substrate. A consequence of this structure is that if the filter is used off-axis, there is a shift of the central wavelength of the filter with angle as described by [34]:

$$\lambda_f = \lambda_0 \left(1 - \left(n_0/n_f\right)^2 \sin^2\theta\right)^{1/2} \tag{7}$$

where λ_f is the center wavelength when the filter is tilted, λ_0 is the center wavelength when it is on axis, known as the design wavelength, n_0 is the refractive index of the external environment (≈ 1 in air), n_f is the effective refractive index of the filter and θ is the angle of incidence. When the angle of incidence increases from zero, the center wavelength decreases below the design wavelength.

Commercially available laser-line filters are generally designed to work with a specific laser and so transmission spectra tend to correspond to existing laser wavelengths. At the time of writing there was no filter available in the 340 nm range desired for this system. The closest filters available from stock were a 325 nm filter (Edmund NT47-612), corresponding to a HeCd laser line, and a 355 nm filter (Edmund NT64-240), corresponding to a Nd:YAG laser line.

A custom laser-line filter was therefore obtained (Horiba Scientific, 339.5NB3), designed specifically for this system. It had a central wavelength of 339.5 nm, matching the $2^1_0 4^1_0$ formaldehyde absorption peak and suitable for the detection

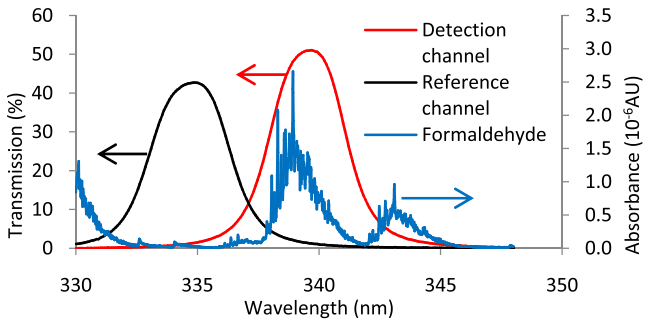

Fig. 3. Transmission spectra of the detection and reference channels of the two-filter system compared to the formaldehyde spectrum from Fig. 1. Filter transmission data was taken using a UV CCD spectrometer (AvaSpec-3648).

channel. The filter had a FWHM of 3.5 nm and a peak transmission of 51%. By tilting a second filter at 14°, the central wavelength could be tuned in accordance with (7) to give a peak wavelength of 335 nm, making it suitable for the reference channel. Fig. 3 shows the transmission spectra of the two channels taken with a UV spectrometer (Avantes AvaSpec-3648, Czerny-Turner configuration, 200 – 1,100 nm spectral range, 0.05 nm spectral resolution) placed in the positions of the photodiodes (See Fig. 2).

The total absorbance of these channels was found by calculating the absorbance at each wavelength using formaldehyde absorption cross-section data from Meller and Moortgat [32]. Assuming a 1 ppm concentration of formaldehyde, the calculated absorbance was 1.33×10^{-5} AU for the detection channel and 1.69×10^{-6} AU for the reference channel. As expected, the detection channel gives a larger absorbance than the reference channel. The detection channel could have given a lower absorbance by tuning its position to slightly shorter wavelengths, but at the cost of both filter transmission and LED intensity.

To find the absorbance that would be created by a quantity of gas, the intensity recorded on the detection and the reference channels was used with (4) and (6). As a small level of absorbance persisted on the reference channel, this had the effect of decreasing the measured normalized absorbance S, from 1.33×10^{-5} AU, by a factor of $(1.33\times10^{-5}$ / $(1.33\times10^{-5} - 1.69\times10^{-6}) = 1.15$. Hence the system was estimated to have a total absorbance of 1.2×10^{-5} AU for 1 ppm of formaldehyde.

The simulation makes a number of assumptions that may not be correct in practice: that the source emission and transmission of other components are spectrally flat and therefore don't distort the filter passbands; that there is minimal off-axis light passing through the filters, which would otherwise slightly broaden and shift the filter passbands; that the formaldehyde spectrum we used had minimal errors on the baseline. For this reason, it would be unwise to rely on the simulation and calibration of the final sensor is required.

C. Electronic Configuration

A schematic diagram of the electronic configuration of the system is shown in Fig. 4. A simplified optical diagram is included in this diagram for reference, the full version of

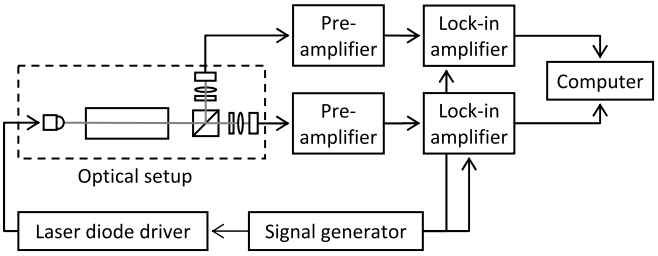

Fig. 4. Diagram of the electronic setup used for the two-filter system.

TABLE I
SUMMARY OF SELECTED ELECTRONIC SETTINGS

Signal generator (Hewlett-Packard 33120a)	
Frequency	Square wave 6.5 kHz
Voltage	8.00 Vpp
laser diode driver (Thorlabs LDC200CV)	
DC Current	9.41 mA
Variable gain amplifiers (FEMTO Messtechnik DLPCA-200)	
Detection channel gain	$\times10^6\ \Omega$
Reference channel gain	$\times10^7\ \Omega$
Lock-in amplifiers (Stanford Research Systems SR850)	
Integration time	10 ms
Gain setting	200 mV

which can be found in Fig. 2. A signal generator was used to provide a square-wave modulation at frequency f and a laser diode driver controlled the current to the LED. The lock-in amplifiers recovered the modulated signals at 1f. A summary of the selected settings is given in TABLE I.

The voltage read by the lock-in amplifiers was recorded by the computer and a LabVIEW interface was used which allowed for some post processing. Specifically, a moving average was taken over two hundred measurements (2s). A rectangular moving average was used, wherein equal weight was given to all values within the measurement window.

IV. NOISE OPTIMIZATION AND CHARACTERIZATION

The main sources of noise are summarized in TABLE II, together with the methods used to control or limit them. NEA values for the optimized performances are given for each using the gain from the photodiodes and generally calculated over a 20 s measurement period.

The current used to drive the LED was a square waveform produced by the signal generator, used to modulate the LED and provide a reference for the lock-in amplifiers. Background electronic noise from the detectors and amplifiers was measured unmodulated with the optical beam blocked, using an electronic spectrum analyser (Stanford Research Systems SR780). A modulation frequency of 6.5 kHz was found to minimise this background noise while also allowing a suitably high gain in the detector amplifiers.

Source fluctuation noise is caused by the random distribution of photons emitted by the LED and follows a Poisson distribution in the rate of detected photons resulting in white noise whose level is shown in TABLE II. Its effect can be decreased by using increased averaging periods.

TABLE II
SUMMARY OF NOISE SOURCES AFFECTING THE SYSTEM

Phenomenon	Initial level	Control	Final level	NEA
Detector / amp electronic noise	Up to 8.4×10^{-5} V/√Hz	Modulation frequency set to 6.5kHz	3.5×10^{-6} V/√Hz	2.4×10^{-5} AU
Thermal drift	Up to 1.5×10^{-6} V/√Hz	Allow system to reach thermal equilibrium	5.2×10^{-8} V/√Hz	7.4×10^{-6} AU over 20s
Lock-in amp output digitisation	7×10^{-5} V	Most averaging performed by computer	3.5×10^{-7} V	1.8×10^{-6} AU
Lock-in amp random noise	4.3×10^{-7} V/√Hz	N/A	4.3×10^{-7} V/√Hz	3.0×10^{-6} AU over 20s
Source fluctuation noise	5.4×10^{-6} V/√Hz	Averaging over 20s	5.4×10^{-6} V/√Hz	3.8×10^{-5} AU over 20s
Total noise based on the above analysis over a 20 s period			6.5×10^{-6} V/√Hz	4.6×10^{-5} AU

Initially a Peltier module and thermocouple were used to control the LED temperature. However, it was found that allowing the LED and filter to reach thermal equilibrium in a temperature-stable room gave a more stable output, a process that took around 2 hours. Packaging the LED with a Peltier element inside the device housing, as is standard practice for many tunable lasers, would improve its temperature control.

Lock-in amplifier digitisation was limited by the 16 bit precision of the output digitiser. A technique was devised for improving the performance of the lock-in amplifiers beyond this digitisation limit. By decreasing the integration time of the lock-in amplifier to 10 ms, random noise (for example electronic noise and source fluctuation) was no longer averaged out and rose to a level where the noise on the output from the lock-in amplifier was significantly greater than the digitisation limit. The noisy output was transferred to a computer and subsequently averaged over 20 s so as to reduce the effects of the random noise. Compared to longer lock-in amplifier averaging, this resulted in a similar level of random noise reduction, over a similar averaging timescale, but with much better precision, avoiding the effects of the digitisation limit.

Lock-in amplifier random noise was determined as the difference between recorded signals when the two lock-in amplifiers were used to measure the same electronic signal. To investigate this, the output of the modulated LED was recorded with a single photodiode and the resulting current was converted to voltage by a single gain amplifier. The voltage signal was then simultaneously recorded by two lock-in amplifiers using the same drive frequency source and the same settings. The noise recorded was attributed to noise from the internal electronics of the lock-in amplifier. As with source fluctuation noise, this random noise source could be decreased by averaging over multiple measurements.

The most significant noise sources identified for this system were thermal drift, predominantly of the LED, and source fluctuation noise. For a single 20 s measurement, source fluctuation and electronic noise dominate, giving a minimum

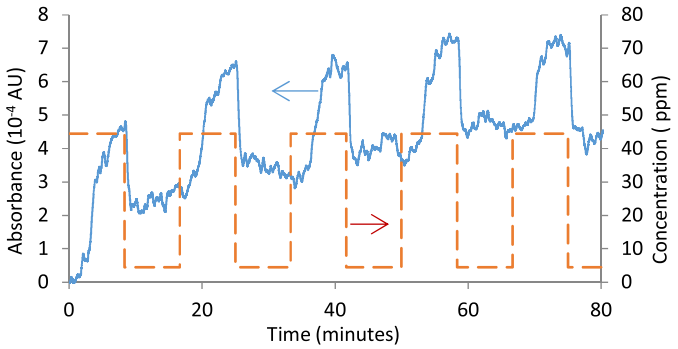

Fig. 5. Absorbance detected by the system (blue solid line) caused by a periodic change in formaldehyde concentration between 4.4 ppm and 44 ppm (red dashed line). The equivalent absorbance change can clearly be seen above the base-line.

detectable absorbance of 4.6×10^{-5} AU, equivalent to a limit of detection of 4.0 ppm of formaldehyde. After approximately 2 minutes, thermal drift increased to similar levels, and over longer measurement periods it would be expected to dominate.

V. FORMALDEHYDE TESTING

The system was tested using formaldehyde generated with a vapour generator (Owlstone Vapor Generator OVG-4) which used a calibrated permeation tube containing para-formaldehyde. The tube was heated to 100 °C to generate a constant, known flux of formaldehyde vapour from the tube. Passing zero air over the tube at a known rate then provided a known formaldehyde concentration. The concentration could be varied either by changing the flow rate over the tube or by downstream dilution with further zero air.

In the first test, to minimise disturbance of the apparatus, the air flow rate was switched between 500 cm^3min^{-1} and 50 cm^3min^{-1}, which yielded concentrations of 4.4 ppm and 44 ppm respectively, giving a total difference of 40±7 ppm. The air flow was switched over five times during the experiment, thus modulating the concentration. The results are shown in Fig. 5.

In Fig. 5 the effect of formaldehyde is an increase in absorbance correlating with the increases in formaldehyde concentration. This verifies that 40 ppm was well above the short-term limit of detection (LoD) of the system. The measured change in absorbance, of approximately 3.5×10^{-4} AU for a 40 ppm change in concentration, is lower than the estimated (simulated) figure of 4.8×10^{-4} AU (Section III.C). A significant variation in the baseline was also observed. It is attributed to poor thermal stability of the LED, which causes a spectral shift in its output, and thermal shifts of the bandpass filters, both of which are investigated in more detail in section VI. Although our system employed a low numerical aperture through the gas cell and filters, it is possible that off-axis beams were present that resulted in slight shifts in the central frequency of the filters and slightly increased bandwidths, beyond the assumptions made in the simulation.

By measuring changes in the baseline deviation from one measurement to the next, the short-term limit of detection (20 seconds) was estimated at around 5×10^{-5} AU or 4.3 ppm

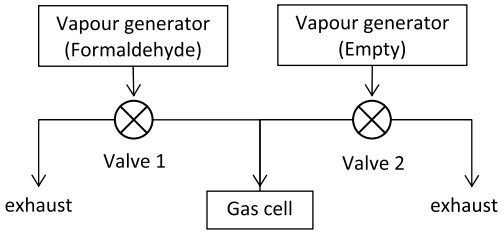

Fig. 6. Formaldehyde delivery system. The two vapour generators supplied air samples at the same flow rate and temperature. One delivered a chosen concentration of formaldehyde, the other, clean air. The supply to the gas cell could be switched between the two without varying the total flow rate.

of formaldehyde. This compares well with our estimated limits of detection of 4.6×10^{-5} AU (TABLE II) and 4.0 ppm. However, the results also show a baseline drift increasing the practical limit of detection to approximately 2×10^{-4} AU. Baseline drift over the 80 minute period of the experiment was consistent with thermal drift over these timescales.

The maximum detectable concentration was not tested due to safety considerations associated with high levels of formaldehyde. However a theoretical maximum sensitivity can be estimated using the known nonlinearity of (1). A reasonable upper limit would be 1 AU, equivalent to 8.6 %vol, giving a dynamic range of 4.3 ppm to 8.6 %vol.

As expected, the results also show that the system responded relatively slowly to the introduction of the highest concentration of formaldehyde, since this was generated using the lowest flow rates of 50 $cm^3 min^{-1}$, filling a cell whose volume was estimated to be 204 cm^3. The signal changed more rapidly on introduction of the lowest concentration, with a flow rate of 500 $cm^3 min^{-1}$.

The main disadvantage of this test method is that the change in total flow rates may have affected the results. Also the concentration could only be decreased to 4.4 ppm, rather than zero, limiting the concentration range of the test. Additional tests were therefore carried out using two vapour generators (both Owlstone Vapor Generator OVG-4) connected as shown in Fig. 6. This allowed the supply to the gas cell to be switched between lines with and without formaldehyde without varying the flow rate, although care had to be taken to switch the two valves at the same time. For each test, the formaldehyde concentration generated by the first vapour generator was controlled by adjusting the temperature of the permeation tube.

The system was tested in this manner with a range of formaldehyde concentrations. The results are shown in Fig. 7, the latter determined using the permeation tube calibration, temperature and flow rate. This shows a clear increase in detected absorbance with increasing concentration above the limit of detection and little or no correlation below it, as expected. As a consequence of the need to leave 500 s (8 minutes) between baseline and detection measurements, which allowed the gas cell to fill, the LoD increased to 2.0×10^{-4} AU or 17 ppm, which was attributed to thermal drift. The position of the estimated limit of detection is marked on the graph. Calculating the expected limit of detection from the system with thermal drift over 500 s gives a limit of detection of 2.2×10^{-4} AU, close to the observed results.

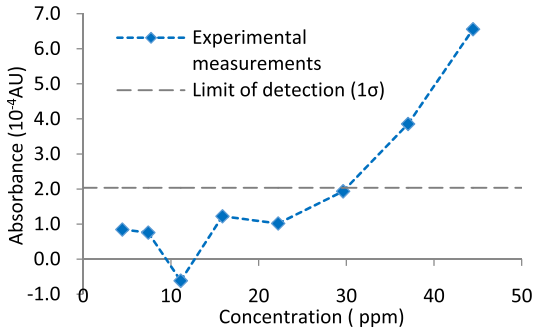

Fig. 7. Graph of the response of the two filter system versus formaldehyde concentration. The position of the estimated limit of detection is shown.

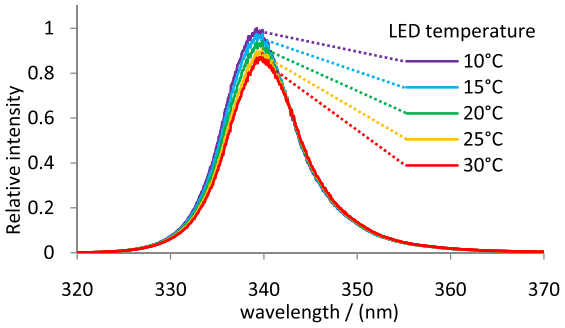

Fig. 8. Output spectrum of the LED changing with temperature, as measured by counts on a UV spectrometer (AvaSpec-3648), normalized relative to the maximum intensity at 10 °C.

VI. Investigation of Thermal Drift

Thermal drift was considered to be the dominant limitation over timescales of more than approximately one minute and was investigated in greater depth by measuring the effects of temperature variation of the LED and interference filters. Several studies have shown an increase in LED peak wavelength with increasing temperature [35]–[37]. This shift would result in a change in the ratio of the detection and reference wavelength bands, potentially causing spurious (positive or negative) absorbance measurements. It is also well-known that temperature changes will affect the transmission of optical interference filters, such that an increase in temperature will increase the peak transmission wavelength.

A. Measurement of LED and Filter Thermal Characteristics

The temperature behaviour of the LED was tested from 10 to 30 °C in an environmental chamber and the results are shown in Fig. 8. The output was recorded using a UV spectrometer (AvaSpec-3648 CCD UV spectrometer). As temperature increases, it can be seen that peak wavelength increases and the intensity decreases. The form of the emission spectrum and its variation with temperature are consistent with previous studies [35]–[37].

The transmission of one interference filter was also tested in the environmental chamber at normal incidence, corresponding to the detection channel. At each temperature, measurements were made using the same UV spectrometer (AvaSpec-3648) both with and without the filter, the entire measurement apparatus being held at the same controlled temperature within the

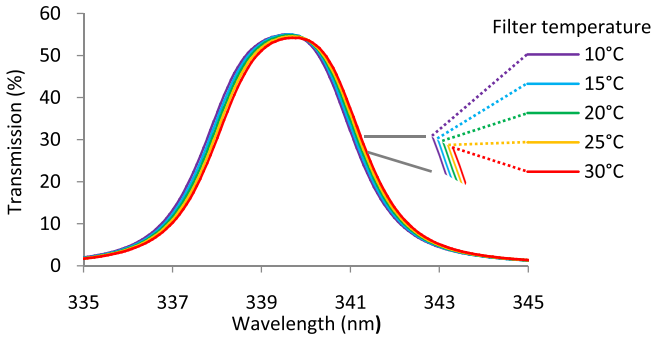

Fig. 9. Transmission spectrum of the detection filter at different temperatures, measured using the UV LED as a source and a UV spectrometer (AvaSpec- 3648).

environmental chamber and allowed to thermally equilibrate prior to measurement. Thus, changes to the LED emission with temperature were normalized out, such that the results in Fig. 9 reveal the effects of temperature on the filter transmission alone. There is a small increase in peak transmission wavelength with increasing temperature as would be expected, of the level of 10 pm $°C^{-1}$, and a small change in transmission level of around -0.04 % $°C^{-1}$.

B. Simulated Effect of Temperature on Formaldehyde Measurements

In order to assess the effect of these temperature changes on the system, the absorbance of the two channels was simulated numerically. The following effects were simulated: thermal drift of the LED and thermal drift of the filters, each with zero gas and in the presence of gas. Over the wavelength range 320-360 nm, the amount of light that would be transmitted through each filter, as I_D and I_R respectively, was calculated according to (4), thus taking into account the LED emission envelope $E_s(\lambda)$ shown in Fig. 8, and the filter transmission $T(\lambda)$, one example being shown in Fig. 9. The final value of S was calculated according to (6). The simulation was performed for chosen concentrations of 0 ppm and 1 ppm, calculated using the spectrum in Fig. 1. The calculations were normalized to a temperature of 20 °C, this being the simulated temperature at which the system was both calibrated and zeroed, thus providing the values of I_{0R} and I_{0D} in (6).

The effect of thermal shifts of the LED was simulated with respect to filters that remained at a fixed temperature of 20 °C. The first simulation was performed for a zero gas condition, and the results are shown in Fig. 10. At lower temperatures, the LED emission increased by a greater amount on the reference channel than on the detection channel, thus (according to (6)) there was an apparent increase in relative absorption and a spurious signal equivalent to the presence of formaldehyde. At temperatures higher than 20 °C the reverse held, with LED emission reduced by more on the reference channel than on the detection channel. Thus, at higher temperatures there was an apparent decrease in relative absorption and the spurious signal was equivalent to a negative absorbance or negative concentration of formaldehyde compared to that at 20 °C. Clearly such negative signals are

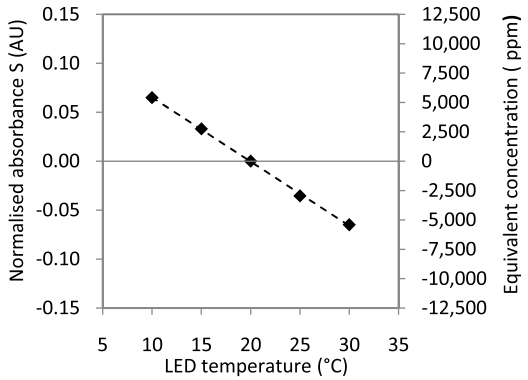

Fig. 10. Simulated effect of changes to the LED temperature on errors in the normalized absorbance and equivalent concentration at zero formaldehyde concentration. The calculation assumes the system has been zeroed and calibrated at 20 °C. The dashed line shows a linear fit to the data.

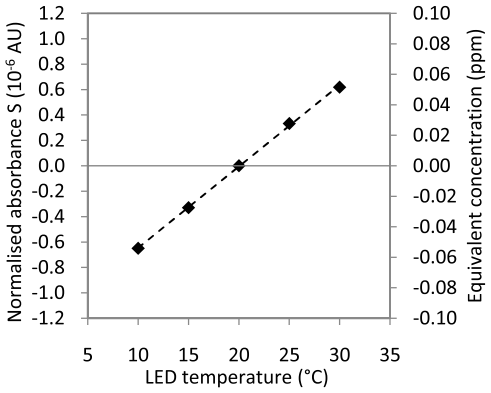

Fig. 11. Simulated effect of changes to the LED temperature on errors in the normalized absorbance and equivalent concentration at 1 ppm formaldehyde concentration. The calculation assumes the system has been zeroed and calibrated at 20 °C, with the baseline error shown in Fig. 10 previously subtracted. The dotted line represents a linear fit to the data.

non-physical, but they would act to mask any true positive absorption signals resulting from real formaldehyde. At zero gas ("zero baseline" condition), the change in spurious signal with LED temperature (Fig. 10) was approximately linear, with a gradient of -6.7×10^{-3} AU $°C^{-1}$ or -560 ppm $°C^{-1}$.

The error in the presence of gas was calculated as follows. First, the value of S was calculated for a simulated concentration of 1 ppm. This was dominated by the change to the zero baseline, therefore to reveal the additional error, the zero gas value of S, taken from Fig. 10, was subtracted. The difference between the baseline-corrected S and the calibrated value of S at 1 ppm then gave the additional error at that concentration, shown in Fig. 12.

At 1 ppm, variations in LED temperature resulted in the zero baseline error of Fig. 10 plus an additional error related to the formaldehyde concentration that was again approximately linear, with a gradient of 6.4×10^{-9} AU $°C^{-1}$ or 5 ppb $°C^{-1}$. Since these absorbances are in the linear region of (1), the errors will be linear with concentration and can therefore also be expressed as a proportional accuracy of the measured signal, namely 0.5 % $°C^{-1}$ in addition to the zero baseline error.

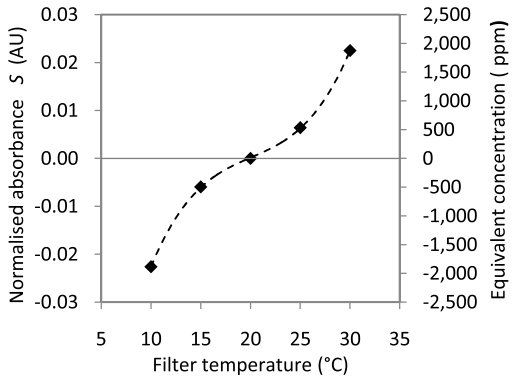

Fig. 12. Simulated effect of change to the temperature of both filters on the normalized absorbance and equivalent concentration of the spurious signal at zero formaldehyde concentration. The calculation assumes the system has been zeroed and calibrated at 20 °C. The dashed line is a visual aid only.

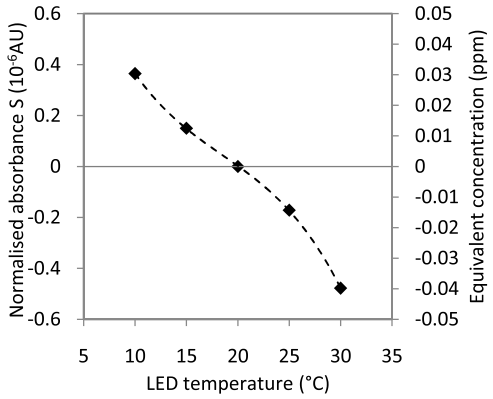

Fig. 13. Simulated effect of changes to the temperature of both filters on the error in the normalized absorbance and equivalent concentration of the spurious signal at 1 ppm formaldehyde concentration. The calculation assumes the system has been zeroed and calibrated at 20 °C, with the baseline error of Fig. 12 previously subtracted. The dashed line is a visual aid only.

Thus, the temperature of the LED has a significant effect on the zero baseline and a smaller additional effect on the proportional accuracy of the signal. To achieve a limit of detection of 4.6×10^{-5} AU therefore implies an LED temperature variation of 7×10^{-3} °C, which explains our difficulties in controlling the LED temperature during experiments. Over longer time periods the limit of 2×10^{-4} AU would have corresponded to a variation of 0.03 °C.

From Fig. 8, we can see that the scale of the problem might be reduced by using only the longer wave LED emission, above the peak wavelength at 30 °C (in this case, above approx. 342 nm) since the change with temperature over this range is much reduced. However, this means using less than half the total LED emission. If the LED peak wavelength could be shortened to below 332 nm, the remaining usable bandwidth would just cover our identified detection and reference channels, but at reduced intensity and with limited tolerance to wavelength variation between devices.

The effect of temperature variation of the filters was calculated in a similar manner. The LED temperature was set to a fixed value of 20 °C and the temperature of the filters was allowed to vary, with the filters assumed to be in good thermal contact, at the same temperature as each other. The results for zero gas are shown in Fig. 12, and the additional error calculated at 1 ppm is shown in Fig. 13.

The effect of temperature variation of the filter was not as profound as that of the LED, but the effect on the zero baseline was nevertheless still high. The effect is highly nonlinear, with more limited variation with temperature around 20 °C (the temperature corresponding to zeroing and calibration) and greater variation below 15 °C or above 25 °C. The effect at zero gas is caused by the relative shift of the filter center wavelengths with respect to the LED emission envelope, which is not flat over the region. The dotted line in Fig. 12 is a polynomial fit to the data included as a visual aid only, with no particular scientific justification. If we assume for simplicity that the region between 15 °C and 25 °C is linear, the change in spurious signal with temperature would be 1.2×10^{-3} AU °C^{-1} or 100 ppm °C^{-1}. For small changes, the reality might be lower.

From Fig. 13, we see the additional error at a concentration of 1 ppm. Again, this is in addition to the larger zero baseline error of Fig. 12 and is revealed once the latter has been subtracted. There is a relative shift in the transmission of the two filters with respect to the target gas absorption, and the effect is nonlinear. Assuming for simplicity that the region between 15 °C and 25 °C is linear, the change in spurious signal with temperature would be -3.2×10^{-8} AU °C^{-1} or -2.7 ppb °C^{-1}. As with the data shown in Fig. 11, we again expect these figures to be linear with concentration and can express this as a proportional accuracy of the measured signal of -0.3 % °C^{-1} in addition to the zero baseline error.

The ideal filter for non-dispersive gas detection is considered to take the form of a "top hat" function, where the cut-off wavelengths allow sufficient tolerance for filter variation caused either by thermal effects or manufacturing tolerances. It may also be possible to reduce the extent of thermal shift of the filter passband, since athermalised narrow bandpass filters are available commercially. Narrow (2.7 nm FWHM) bandpass filters are available in the near IR, for the purpose of dense wavelength division multiplexing across the 1550 nm telecoms band, with a temperature coefficient of 1.5 pm °C^{-1} at 1531 nm [38] (our Fig. 9 shows 10pm °C^{-1}). This level of athermalisation would reduce the effect of thermal changes to the filters on instrument performance, but would come at increased cost.

Temperature variation of both the LED and filters has therefore caused an error in both the zero baseline measurement and measurements made in the presence of gas, the latter being proportional to the gas concentration. Because we are in the linear region of (1), these errors are additive, though the LED and filters may not necessarily be at the same temperature. The error on the zero baseline dominates, which is consistent with the experimental data in Fig. 5, where a large drift in the zero baseline can be seen above the noise level, but the step change in S in response to changes in gas concentration appears to be constant (lower than the noise) throughout.

VII. Discussion and Conclusions

A new method of detecting and measuring formaldehyde has been demonstrated as a first proof of concept, based on a non-dispersive spectroscopic technique in the UV region.

Narrow (3 nm) bandpass filters were used to define detection and reference channels that corresponded to regions of high and low formaldehyde absorption, respectively. Fine tuning of the center wavelength of the filters was achieved by making small changes to the angle of incidence. Light from a single LED was collimated through a gas cell and then divided into the two channels by a beam splitter. The intensity in each channel was measured with a photodiode and the ratio between the detection and reference channels was used to calculate the formaldehyde concentration.

The noise performance of this system was characterised and optimized. Noise phenomena that were identified included interference from frequencies matching the modulation frequency, thermal drift, quantisation, lock-in amplifier noise and source fluctuation noise. After optimization the most significant were source fluctuation noise and thermal drift of the LED, giving a best-case limit of detection of 4.6×10^{-5} AU over a 20 s time period. Based on the absorption spectrum of formaldehyde gas, this was calculated to correspond to 4.0 ppm for our pathlength of 19.5 cm. Experimental results measured with a 20 s integration period confirmed limits of detection of 5.0×10^{-5} AU and 4.3 ppm, respectively. For later tests at lower flow rates, it took approximately eight minutes to change the gas concentration in the cell, and the observed LoD increased to 2.0×10^{-4} AU (17 ppm). This was similar to the expected limit of detection of 2.2×10^{-4} AU from observed thermal drift over that time period.

A series of tests was completed over a range of concentrations. Above the limit of detection, the system gave absorption results with a clear correlation with increased concentration. Below the limit of detection, there was little or no correlation as would be expected. However, the design of the vapour generator limited both the range of test concentrations that could be generated and the experimental timescales, which were considerable (over 8 minutes to flush the gas cell), owing to the need to use a low total flow rate. The limit of detection for these tests was increased by time-dependent drift, considered to be dominated by thermal drift of the LED that resulted in changes to the zero baseline. For this system, the zero baseline uncertainty is dependent on the degree of thermal control that can be achieved, with uncertainty characterized at -560 ppm C^{-1} resulting from thermal instability of the LED, and 100 ppm $°C^{-1}$ arising from thermal instability of the filters. An additional error was calculated for measurements in the presence of gas, corresponding to a proportional accuracy of 0.5 % $°C^{-1}$ and -0.3 % $°C^{-1}$ for thermal instability of the LED and filters respectively, in addition to the zero baseline error. This area therefore requires significant improvement for a sensor to be capable of measuring concentrations at the level of 0.1 ppm.

The system required calibration based on the specific arrangement and properties of the filters, LED and other optical components. If different aging or contamination effects were to occur over time, the system would require re-zeroing and/or re-calibration. This is an issue that potentially affects other non-dispersive systems and has not, for example, prevented the commercial uptake of non-dispersive infrared sensors.

A future system could be improved with a thermo-electric controller (TEC) element placed closer to the LED. This would preferably be inside the device package and installed at the time of manufacture, as is standard practice for many tunable diode lasers and some mid IR LEDs. Small (9 mm diameter) integrated devices are available for non-dispersive infrared (NDIR) detection that combine multiple detection channels, each with its own bandpass filter; the same arrangement would also benefit this application. Additionally, a gas cell with a longer pathlength, potentially with multiple light passes, would increase sensitivity. A number of design compromises were also made, whose avoidance would also improve the system's potential. These include the fact that the reference filter's transmission was lowered and its passband broadened as a consequence of its tilt, and also the fact that the LED emission was not ideally centered over measurement channels used. Thermal stability would be improved by a second custom filter for the reference band, with a peak transmission at 335 nm, plus an LED whose peak emission was blue-shifted to below 332 nm. As detector noise is a key contributor to system performance, increasing the intensity of light received by the detectors would also be beneficial. Although blue-shifting the LED would reduce the usable light from this source on the detection band, the rapid development in UV LED technology that is taking place at the present time could result in greater overall intensities on both channels.

We might ask, what are the requirements for sub - ppm formaldehyde detection using this technique? To support the 0.1 ppm action level for indoor air quality recommended by the WHO as a limit of quantification, a limit of detection (1σ) of 10 ppb would likely be needed. If the LED temperature could be controlled to 0.01 °C (the precision of many commercially available controllers), a limit of detection of 1.3 ppm formaldehyde would be expected with the current system. This would be improved by only using the longer wavelength portion of the emission, perhaps by a factor of 10, to approximately 130 ppb. A pathlength increase to 2.5 m would then be needed to provide a 10 ppb limit of detection. This might be achieved with a suitable multipass cell, but at increased cost and complexity of the system and with a negative consequence for the received light intensity. A further question is whether temperature control of the filters would be required, which is not currently an option on commercially available integrated photodetector / filter combinations used in non-dispersive infrared detection. With an athermal design that has closer to a "top hat" bandpass function, thermal instability might be reduced to the level where active control was not required. Temperature compensation, rather than control, might be achieved using a thermistor located on the detector and a look-up table to correct the results.

To summarise, we have demonstrated non-dispersive ultraviolet detection of formaldehyde at ppm levels. The system has the advantage of using a limited number of simple components including a UV LED, narrow bandpass filters and silicon photodetectors, thus avoiding the use of a UV spectrometer. We have completed a comprehensive analysis of the system's performance limitations, concluding that the instrument is currently limited by thermal drift of the UV LED source.

Further work is required to address a number of engineering compromises and limitations in order for the instrument to provide useful measurements with a detection limit of 10 ppb, for the purpose of indoor air quality monitoring.

VIII. Acknowledgment

Data underlying this study can be accessed through the Cranfield University repository at https://doi.org/10.17862/cranfield.rd.4766023.

References

[1] Y. Lu, J. Liu, B. Lu, A. Jiang, and C. Wan, "Study on the removal of indoor VOCs using biotechnology," *J. Hazardous Mater.*, vol. 182, nos. 1–3, pp. 204–209, 2010.

[2] S. Kim, "Control of formaldehyde and TVOC emission from wood-based flooring composites at various manufacturing processes by surface finishing," *J. Hazardous Mater.*, vol. 176, nos. 1–3, pp. 14–19, 2010.

[3] G. D. Nielsen and P. Wolkoff, "Cancer effects of formaldehyde: A proposal for an indoor air guideline value," *Arch. Toxicol.*, vol. 84, no. 6, pp. 423–446, 2010.

[4] C. Persoz, S. Achard, C. Leleu, I. Momas, and N. Seta, "An *in vitro* model to evaluate the inflammatory response after gaseous formaldehyde exposure of lung epithelial cells," *Toxicol. Lett.*, vol. 195, nos. 2–3, pp. 99–105, 2010.

[5] F. Röck, N. Barsan, and U. Weimar, "System for dosing formaldehyde vapor at the ppb level," *Meas. Sci. Technol.*, vol. 21, no. 11, p. 115201, 2010.

[6] H. Kudo, Y. Suzuki, T. Gessei, D. Takahashi, T. Arakawa, and K. Mitsubayashi, "Biochemical gas sensor (bio-sniffer) for ultrahigh-sensitive gaseous formaldehyde monitoring," *Biosensors Bioelectron.*, vol. 26, no. 2, pp. 854–858, 2010.

[7] T. Salthammer, S. Mentese, and R. Marutzky, "Formaldehyde in the indoor environment," *Chem. Rev.*, vol. 110, no. 4, pp. 2536–2572, 2010.

[8] T. Jiang, D. J. Gardner, and M. G. D. Baumann, "Volatile organic compound emission arising from the hot-pressing of mixed-hardwood particleboard," *Forest Products J.*, vol. 52, no. 11, pp. 66–67, 2002.

[9] M. Risholm-Sundman, A. Larsen, E. Vestin, and A. Weibull, "Formaldehyde emission—Comparison of different standard methods," *Atmos. Environ.*, vol. 41, no. 15, pp. 3193–3202, 2007.

[10] A. Al-Hemoud, L. Al-Awadi, M. Al-Rashidi, K. A. Rahman, A. Al-Khayat, and W. Behbehani, "Comparison of indoor air quality in schools: Urban vs. Industrial 'oil & gas' zones in Kuwait," *Building Environ.*, vol. 122, pp. 50–60, Sep. 2017.

[11] J. C. S. Chang, R. Fortmann, N. Roache, and H.-C. Lao, "Evaluation of low-VOC latex paints," *Indoor Air*, vol. 9, no. 4, pp. 253–258, 1999.

[12] M. Nicolas, O. Ramalho, and F. Maupetit, "Reactions between ozone and building products: Impact on primary and secondary emissions," *Atmos. Environ.*, vol. 41, no. 15, pp. 3129–3138, 2007.

[13] X. Liu, M. A. Mason, Z. Guo, K. A. Krebs, and N. F. Roache, "Source emission and model evaluation of formaldehyde from composite and solid wood furniture in a full-scale chamber," *Atmos. Environ.*, vol. 122, pp. 561–568, Dec. 2015.

[14] PPM Technology Ltd. *Formaldemeter Htv*. Accessed: 2016. [Online]. Available: http://www. ppm-technology.com/formaldemeter%20htv.htm

[15] D. Z. Chen and Y. J. Yuan, "Thin-film sensors for detection of formaldehyde: A review," *IEEE Sensors J.*, vol. 15, no. 12, pp. 6749–6760, Dec. 2015.

[16] J. Hodgkinson and R. P. Tatam, "Optical gas sensing: A review," *Meas. Sci. Technol.*, vol. 24, no. 1, p. 012004, 2013.

[17] G. Wysocki *et al.*, "Dual interband cascade laser based trace-gas sensor for environmental monitoring," *Appl. Opt.*, vol. 46, no. 33, pp. 8202–8210, 2007.

[18] D. Richter, A. Fried, B. P. Wert, J. G. Walega, and F. K. Tittel, "Development of a tunable mid-IR difference frequency laser source for highly sensitive airborne trace gas detection," *Appl. Phys. B, Lasers Opt.*, vol. 75, nos. 2–4, pp. 281–288, 2002.

[19] H. Barry, L. Corner, G. Hancock, R. Peverall, and G. A. D. Ritchie, "Cross sections in the $2\nu_5$ band of formaldehyde studied by cavity enhanced absorption spectroscopy near 1.76μm," *Phys. Chem. Chem. Phys.*, vol. 4, pp. 445–450, Jan. 2002.

[20] M. Angelmahr, A. Miklós, and P. Hess, "Photoacoustic spectroscopy of formaldehyde with tunable laser radiation at the parts per billion level," *Appl. Phys. B, Lasers Opt.*, vol. 85, nos. 2–3, pp. 285–288, 2006.

[21] M. Horstjann *et al.*, "Formaldehyde sensor using interband cascade laser based quartz-enhanced photoacoustic spectroscopy," *Appl. Phys. B, Lasers Opt.*, vol. 79, no. 7, pp. 799–803, 2004.

[22] Gasera product brochure, Gasera, Turku, Finland. *Gasera One, Formaldehyde*. Accessed: 2016. [Online]. Available: http://www.gasera.fi/product/gasera-one-formaldehyde-photoacoustic-gas-analyzer/

[23] O. V. Postylyakov, A. N. Borovski, V. A. Ivanov, A. V. Dzhola, E. I. Grechko, and Y. Kanaya, "Formaldehyde integral content in troposphere of Moscow region: Preliminary results of 6 years of measurements using DOAS technique," *Proc. SPIE.*, vol. 10035, Nov. 2016, Art. no. 10035A.

[24] W. Thomas, E. Hegels, S. Slijkhuis, R. Spurr, and K. Chance, "Detection of biomass burning combustion products in Southeast Asia from backscatter data taken by the GOME Spectrometer," *Geophys. Res. Lett.*, vol. 25, no. 9, pp. 1317–1320, 1998.

[25] I. De Smedt, J. F. Müller, T. Stavrakou, R. A. Van Der, H. Eskes, and M. Van Roozendael, "Twelve years of global observations of formaldehyde in the troposphere using GOME and SCIAMACHY sensors," *Atmos. Chem. Phys.*, vol. 8, no. 16, pp. 4947–4963, 2008.

[26] F. Wittrock *et al.*, "Simultaneous global observations of glyoxal and formaldehyde from space," *Geophys. Res. Lett.*, vol. 33, no. 16, 2006, Art. no. L16804.

[27] J. Stutz and U. Platt, "Numerical analysis and estimation of the statistical error of differential optical absorption spectroscopy measurements with least-squares methods," *Appl. Opt.*, vol. 35, no. 30, pp. 6041–6053, 1996.

[28] M. Hausmann, U. Brandenburger, T. Brauers, and H.-P. Dorn, "Simple Monte Carlo methods to estimate the spectra evaluation error in differential-optical-absorption spectroscopy," *Appl. Opt.*, vol. 38, no. 3, pp. 462–475, 1999.

[29] R. A. Washenfelder, A. R. Attwood, J. M. Flores, K. J. Zarzana, Y. Rudich, and S. S. Brown, "Broadband cavity-enhanced absorption spectroscopy in the ultraviolet spectral region for measurements of nitrogen dioxide and formaldehyde," *Atmos. Meas. Tech.*, vol. 9, pp. 41–52, 2016.

[30] J. J. Davenport, J. Hodgkinson, J. R. Saffell, and R. P. Tatam, "A measurement strategy for non-dispersive ultra-violet detection of formaldehyde in indoor air: Spectral analysis and interferent gases," *Meas. Sci. Technol.*, vol. 27, no. 1, p. 015802, 2016.

[31] J. D. Ingle and S. R. Crouch, *Spectrochemical Analysis*. Englewood Cliffs, NJ, USA: Prentice-Hall, 1988.

[32] R. Meller and G. K. Moortgat, "Temperature dependence of the absorption cross sections of formaldehyde between 223 and 323 K in the wavelength range 225–375 nm," *J. Geophys. Res.-Atmos.*, vol. 105, no. D6, pp. 7089–7101, 2000.

[33] D. J. Clouthier and D. A. Ramsay, "The spectroscopy of formaldehyde and thioformaldehyde," *Annu. Rev. Phys. Chem.*, vol. 34, pp. 31–58, Oct. 1983.

[34] *Edmund Optics NT64-240, Technical Data Sheet*, Edmund Opt. Inc., Barrington, NJ, USA.

[35] Y. Xi *et al.*, "Junction and carrier temperature measurements in deep-ultraviolet light-emitting diodes using three different methods," *Appl. Phys. Lett.*, vol. 86, p. 031907, 2005.

[36] K. J. Reynolds, J. P. De kock, L. Tarassenko, and J. T. B. Moyle, "Temperature dependence of led and its theoretical effect on pulse oximetry," *Brit. J. Anaesthesia*, vol. 67, no. 5, pp. 638–643, Nov. 1991.

[37] J.-C. Wang *et al.*, "The effect of junction temperature on the optoelectrical properties of InGaN/GaN multiple quantum well light-emitting diodes," *J. Lumin.*, vol. 132, no. 2, pp. 429–433, 2012.

[38] Iridian Spectral Technologies Ltd, Ottawa, ON, Canada. (2017). *DWDM 100 GHz 4s0*. Accessed: Mar. 15, 2017. [Online]. Available: https://www.iridian-optical-filters.com/product/dwdm-100-ghz-4s0-1531-507/

J. J. Davenport received the M.Sc. degree in physics and the M.Sc. degree in photonics from Imperial College London in 2010, and the Ph.D. degree in engineering photonics from Cranfield University in 2014. He is currently a Research Associate in biomedical engineering with the City, University of London. His research to date focuses on spectroscopic detection and analysis of gases in complex environments such as industrial buildings or the human body, specifically on sensitivity and specificity optimization.

J. Hodgkinson received the B.A. degree in natural sciences from the University of Cambridge in 1989, and the Ph.D. degree from the Optoelectronics Research Centre, University of Southampton, in 1998. She is currently a Senior Lecturer in applied photonics with Cranfield University. After a career in the chemical, water and gas industries, she joined Cranfield in 2004, funded by an EPSRC Advanced Research Fellowship (2004–2010). Her research into optical gas sensing encompasses non-dispersive optical detection, tunable diode laser spectroscopy, and optical fiber sensing. She is Chair of the Gas Analysis and Sensing Group, a U.K. technology forum for all aspects of gas sensing and measurement.

J. R. Saffell received the B.Sc. degree in chemistry from MIT in 1975 and the Ph.D. degree in materials science from Cambridge University in 1979. He has been the Technical Director of Alphasense Ltd., since 1997. He has been involved in gas sensing and water quality measurement for 30 years and is responsible for working with Universities to develop and exploit new gas sensing technologies. He is the Chairman of the U.K. Council of Gas Detection and Environmental Measurement and previous Chairman of the U.K. Sensors for Water Interest Group.

R. P. Tatam received the B.Sc. degree in chemistry and physics from the University of Exeter in 1981 and the Ph.D. degree in physics from the City of London Polytechnic in 1986. He worked in the Physics Laboratory of the University of Kent before joining Cranfield in 1989, where he is currently a Professor of Engineering Photonics and the Head of the Centre for Engineering Photonics. He has published over 450 papers. His research aims to develop novel optical instrumentation to better understand physical phenomena, and encompasses optical fibre sensors, speckle interferometry, laser Doppler anemometry, optical coherence tomography, and gas sensing. He was a recipient of D.Sc. from the University of Exeter, is a Fellow of SPIE, and was elected to its Board of Directors (2010–2012).

Non-dispersive ultra-violet spectroscopic detection of formaldehyde gas for indoor environm

Davenport, J. J.

2018-01-25

Davenport JJ, Hodgkinson J, Saffell JR, Tatam RP. (2018) Non-dispersive ultra-violet spectroscopic detection of formaldehyde gas for indoor environments. IEEE Sensors Journal, Volume 18, issue 6, March 2018, pp. 2218-2228

http://dx.doi.org/10.1109/JSEN.2018.2795042